Resolving quandaries surrounding NiTi

Jifeng Wang and Huseyin Sehitoglu

Citation: Appl. Phys. Lett. **101**, 081907 (2012); doi: 10.1063/1.4747488
View online: http://dx.doi.org/10.1063/1.4747488
View Table of Contents: http://apl.aip.org/resource/1/APPLAB/v101/i8
Published by the American Institute of Physics.

Related Articles

High cyclic stability of the elastocaloric effect in sputtered TiNiCu shape memory films
Appl. Phys. Lett. 101, 091903 (2012)

Deformation induced martensite in NiTi and its shape memory effects generated by low temperature laser shock peening
J. Appl. Phys. 112, 033515 (2012)

Martensitic transformation and magnetic domains in Mn50Ni40Sn10 studied by in-situ transmission electron microscopy
J. Appl. Phys. 112, 033904 (2012)

Variation of magnetic domain structure during martensite variants rearrangement in ferromagnetic shape memory alloys
Appl. Phys. Lett. 101, 032401 (2012)

Magnetostriction in the vicinity of structural transitions in Ni2MnGa
Appl. Phys. Lett. 100, 262410 (2012)

Additional information on Appl. Phys. Lett.

Journal Homepage: http://apl.aip.org/
Journal Information: http://apl.aip.org/about/about_the_journal
Top downloads: http://apl.aip.org/features/most_downloaded
Information for Authors: http://apl.aip.org/authors

ADVERTISEMENT

Resolving quandaries surrounding NiTi

Jifeng Wang and Huseyin Sehitoglu[a)]
Department of Mechanical Science and Engineering, University of Illinois, 1206 West Green Street, Urbana, Illinois 61801, USA

(Received 29 June 2012; accepted 8 August 2012; published online 22 August 2012)

We address a quandary associated with the phase stability of NiTi. The B19′ (monoclinic lattice) has been experimentally observed while B33 (base-centered orthorhombic lattice) has been proposed on theoretical grounds to have a lower energy. With high-resolution shearing steps, we show unequivocally that a significant energy barrier exists between the martensitic B19′ and B33 which is dependent on pressure. The transition state designated as B19′^{1} has an energy level 25 meV/atom higher compared to B19′. We note that the formation of B33 can be suppressed because of the presence of the B19′^{1} high energy barrier which increases considerably under tensile hydrostatic stress. © *2012 American Institute of Physics*. [http://dx.doi.org/10.1063/1.4747488]

Equiatomic NiTi has been the most widely studied shape memory alloy (SMA) owing to its superior shape memory characteristics.[1] Experimental investigations have revealed that the B19′structure is the martensitic phase in NiTi.[2–4] However, recent DFT calculations[5–9] suggested that the B19′ structure is unstable compared to a higher-symmetry base-centered orthorhombic (BCO) structure (also termed B33 with monoclinic angle $\gamma \approx 107^\circ$). Some of these investigations proposed barrierless transformation paths between the B2 and B19′ as well as from the B19′ to B33 lattices.[6,7,9] But the question remains, why is B19′ experimentally observed? Two major explanations have been proposed in the literature: (1) the B19′ structure is stabilized by internal (or residual) stresses which exist within the microstructure,[8,9] and the B33 structure may be formed in certain conditions when the internal stresses are minimized;[6] (2) it has been proposed that the presence of (nano) twins, often experimentally observed,[10–13] can lower the B19′ energy.[14,15] In addition, we also note that the energy of the self-accommodated (internally twinned) B19′ structure is lower compared to its detwinned counterpart.[1] Another point is that the B33 structure corresponds to a rather high (10.1%) elongation of the largest lattice parameter (compared to 3% (Ref. 6) for B19′); hence there is a corresponding higher elastic strain energy.

In this letter, we provide a more authoritative explanation of the occurrence of B19′ that has been overlooked: there are two energy barriers in the martensitic phase transformation path from the B19′ to B33, and the magnitude of the highest barrier is in the range of 8–25 meV/atom depending on the applied pressure.

We utilized DFT to investigate the phase stability and the corresponding energy barriers over the entire path, which is accomplished by an atomic bilayer shear distortion in the {011} basal plane along the ⟨100⟩ slip direction with structural optimization for all lattice parameters, angles, and internal atomic coordinates.[6,7] The first-principles total-energy calculations were carried out using the Vienna *ab initio* Simulations Package (VASP)[16,17] with the projector augmented wave (PAW) method and the generalized gradient approximation (GGA). PAW is an efficient all-electron method which achieves high accuracy when transition elements such as Ti are considered. In our calculation, Monkhorst-Pack $9 \times 9 \times 9$ k-point meshes were used for the Brillouin-zone integration. Ionic relaxation was performed by a conjugate gradient algorithm and stopped when absolute values of internal forces were smaller than 5×10^{-3} eV/Å. The energy cut-off of 500 eV was used for the plane-wave basis set. The total energy was converged to less than 10^{-5} eV per atom. The equilibrium structures for all phases were obtained by minimizing total energies at zero temperature. Furthermore, to simulate the effect of internal stresses, we calculated structural total energies and energy barriers under several hydrostatic stresses in the range of −14 GPa to 14 GPa. The computed lattice parameters, monoclinic angles, volumes, total energies relative to the B2 phase (considered as the reference state), and energy barriers in the transformation are summarized in Table I (for the 0 GPa and 10 GPa cases).

The present results (B2, B19′, and B33 at zero pressure) are compared with previous theoretical[6,8,18,19] and experimental findings,[2,4,20] and they are in excellent agreement. However, we point to several metastable structures and transition states which have not been discovered before. In this letter, the most important transition state is defined as B19′^{1} (Fig. 1). Our first-principles calculations confirm that the B19′ has higher energy relative to the B33 at zero pressure, while at 10 GPa hydrostatic tension B19′ has the lowest energy. We discovered the energy barrier of 8 meV/atom (corresponding to B19′^{1}) between the B19′ and B33 as the most significant in Fig. 1 (and Table I) which is raised to 25 meV/atom at 10 GPa. We note that all lattice parameters change abruptly after the shear displacement reaches $\frac{u}{a_0} = 0.21$ corresponding to B19′^{1} (see Table I). The decrease of the lattice parameters a (in-plane Ni-Ni interatomic distance between two adjacent {100} layers) and b (in-plane Ni-Ni interatomic distance between two adjacent {011} layers) significantly affects the arrangement of atoms that get closer to each other, which causes excessive interatomic repulsive forces during the shear transformation. As $\frac{u}{a_0} = 0.21$ is approached, the interatomic distances in these layers will increase as shear proceeds, and the total energies will

a)Author to whom correspondence should be addressed. Electronic mail: huseyin@illinois.edu.

TABLE I. VASP-PAW-GGA calculated lattice parameters (Å), monoclinic angle (degree), volume (Å^3 per formula unit), total energies (meV per atom) relative to B2 austenite phase considered as reference state and energy barriers (meV per atom) in the phase transformation of NiTi for two cases: zero pressure, hydrostatic tension at 10 GPa.

	Zero pressure							Hydrostatic tension 10 GPa					
Structures	a	b	c	γ	V	$E-E_{B_2}$	Energy barrier	a	b	c	γ	$E-E_{B_2}$	Energy barrier
B2	3.004	4.25	4.25	90	27.1	0	B2 → B2^1 → B2′	3.07	4.35	4.35	90	0	B2 → B2^1 → B2′
B2′	2.91	4.32	4.31	90.5	27.11	−4.38	*0.53*	2.97	4.43	4.42	90.71	−0.64	*1.76*
B2′^{1}	2.93	4.31	4.27	90.7	26.88	−2.48	B2′ → B2′^{1} → B19′	3.07	4.35	4.34	91.52	1.83	B2′ → B2′^{1} → B19′
B19′	2.91	4.64	4.06	97.3	27.18	−44.1	*2*	3.03	4.77	4.08	101.2	−49.6	*2.47*
		4.58		90.9					4.74		90.52		
B19′^{1}	2.88		4.11		27.24	−36.14		2.99		4.16		−24.5	
		4.67		96.69			B19′ → B19′^{1} → B19″		4.8		96.34		B19′ → B19′^{1} → B19″
B19″	2.94	4.76	3.99	101.7	27.44	−51.37	*8*	3.04	4.87	4.07	102	−43.1	*25*
							B19″ → B19″^{1} → B33						B19″ → B33
B33	2.93	4.91	4.00	107.38	27.51	−52.4		3.05	5.02	4.08	107.7	−39.3	
							0.37						*3.78*

decrease until the B19″ is formed. The metastable structure B19″ results in a very small energy barrier less than 0.4 meV/atom.

A schematic of the bilayer shear transformation from the B2 to B19′^{1} in the {011} basal plane along the ⟨100⟩ slip direction is given in Fig. 2. We note that the B19′^{1} is composed of two monoclinic lattices with different monoclinic angles, $\gamma^{(1)} = 90.9°$ and $\gamma^{(2)} = 96.69°$, and different largest lattice parameters, $b^{(1)} = 4.58$ Å and $b^{(2)} = 4.67$ Å, i.e., a double-monoclinic-hybrid structure. As a non-equilibrium state in the transformation path from the B19′ to B33, this double-monoclinic-hybrid structure connected through a coherent interface is formed by allowing full relaxation of the lattice parameters, monoclinic angles, and atomic positions in the DFT calculation. The full relaxation approach, during the imposed bilayer {011}⟨100⟩ shear, results in a shuffle of the atomic positions and lowers the structural energy during the phase transformation.[6,7] However, the B19′^{1} hybrid structure still constitutes an important energetic barrier which makes the transition to B33 difficult.

The B19′^{1} plays a key role in the phase transformation from the B19′ to B33 as at this transition state we found a significantly high energy barrier of around 8 meV/atom above the B19′ (this is the globally highest cubic-monoclinic energy barrier). Since the energy barriers between the B2 and B2′ (0.53 meV/atom) as well as the B2′ and the B19′ (2 meV/atom) are rather low, the stress required to induce B19′ from B2 is not high. In contrary, the stress required for B19′ to B33 change will be much higher owing to the large energy barrier between them. So even if the B33 is energetically preferred, the transformation from the B2 to the B19′

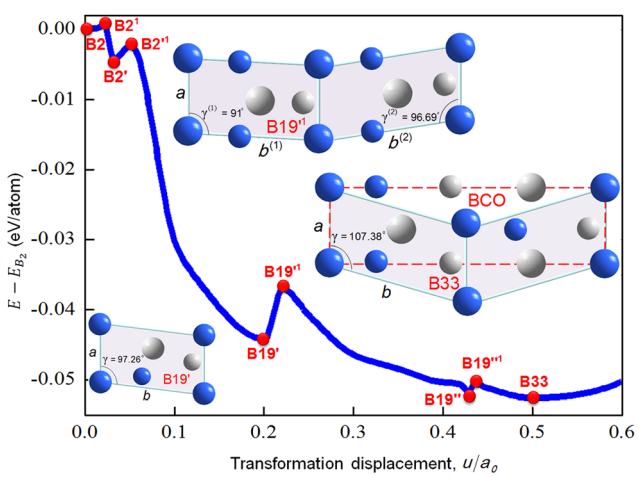

FIG. 1. Total energies variation with the transformation displacement from the B2 to the B33 of NiTi. The B19′^{1} is composed of two monoclinic lattices with 8 atoms (a double-monoclinic-hybrid structure, see Fig. 2 for details). The B33 can be represented in a 4-atom monoclinic unit cell with an angle 107.38° or in an 8-atom base center orthorhombic unit cell (red dash line) related to two equivalent monoclinic unit cells. The blue and grey spheres correspond to Ni and Ti atoms, respectively. The large spheres represent atoms in the plane, and small spheres are located out of plane (one layer below or above) of the unit cells.

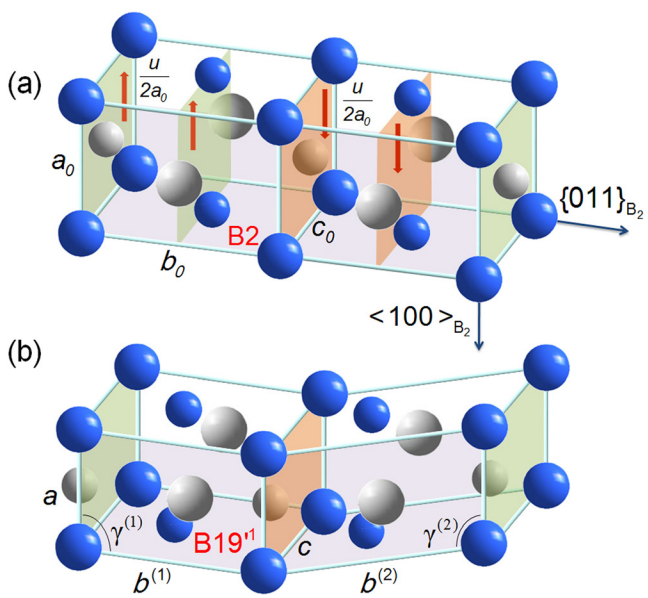

FIG. 2. Schematic of the bilayer shear transformation from B2 to B19′^{1}. (a) The initial B2 structure with lattice parameters a_0, b_0 and c_0. The green and red color planes are the {011} basal planes, which form the sheared bilayers. The red arrows show the alternating shear direction with normalized magnitude $\frac{u}{2a_0}$ in the {011} basal planes. (b) The B19′^{1} structure is formed after relative shear displacement of $\frac{u}{a_0} = 0.21$. It is a double-monoclinic-hybrid structure with different monoclinic angles, $\gamma^{(1)} = 90.9°$ and $\gamma^{(2)} = 96.69°$, and different largest lattice parameters, $b^{(1)} = 4.58$ Å and $b^{(2)} = 4.67$ Å.

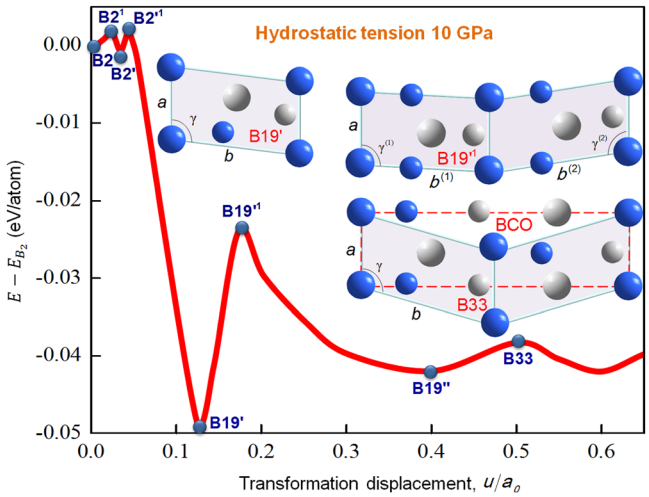

FIG. 3. Effects of hydrostatic tension at 10 GPa on total energies in the phase transformation of NiTi. The energy barrier between the B19′ and B33 is much higher as 25 meV/atom. The B19′ is the global minimum energy structure, and the B33 becomes a transition state in the transformation path.

overcomes a much lower barrier, and the system will be stabilized at the B19′ phase.

The effect of hydrostatic tension at 10 GPa on the structural total energies and energy barriers is shown in Fig. 3. Compared to the result at zero pressure in Fig. 1, the position of the shear levels corresponding to the transformation steps and energy barriers are altered dramatically by pressure. Three major pressure effects are evident: (1) the energy barrier between the B19′ and B33 increases from 8 meV/atom at zero pressure to 25 meV/atom at 10 GPa; (2) the B19′ has lower energy than B33 and becomes the global minimum energy structure, which indicates that the B19′ is more stable than the B33 under hydrostatic tension; (3) the B19′ occurs at a smaller transformation displacement, $\frac{u}{a_0}$, permitting a smaller shear strain to achieve the transformation from B2 to B19′. Overall, the results point to the presence of an energy barrier that is a strong function of applied pressure in NiTi, and the B19′ may become energetically stable relative to the B33 under high hydrostatic tension.

To examine the phase stability of the B19′ relative to B33 at various hydrostatic stresses (negative hydrostatic stress corresponds to positive pressure), we calculated the total energy difference between them as shown in Table II.

TABLE II. Total energy difference between the B19′ and B33 under hydrostatic stress.

Hydrostatic stress (GPa)	−8	0	4	8	10
B19′−B33 (meV/atom)	16.9	8.3	3.4	3.2	−10.3

We note that the total energy difference favors B19′ as the stable structure at 10 GPa of tensile hydrostatic stress.

We conclude that the presence of energy barriers and their magnitude in the martensitic phase transformation of NiTi is central to understanding the stabilization of the observed B19′ structure. The hydrostatic stress influences the structural energies; especially, the high hydrostatic tension can significantly contribute to stabilize the B19′structure in martensite.

The work is supported by the NSF-CMMI grant 09-26813.

[1]T. Ezaz and H. Sehitoglu, Appl. Phys. Lett. **98**, 141906 (2011).
[2]Y. Kudoh, M. Tokonami, S. Miyazaki, and K. Otsuka, Acta Metall. **33**, 2049 (1985).
[3]G. M. Michal and R. Sinclair, Acta Crystallogr. B **37**, 1803 (1981).
[4]S. D. Prokoshkin, A. V. Korotitskiy, V. Brailovski, S. Turenne, I. Y. Khmelevskaya, and I. B. Trubitsyna, Acta Mater. **52**, 4479 (2004).
[5]K. Guda Vishnu and A. Strachan, Acta Mater. **58**, 745 (2010).
[6]N. Hatcher, O. Y. Kontsevoi, and A. J. Freeman, Phys. Rev. B **80**, 144203 (2009).
[7]J. Morris, K. Maja, and F. Chong, Mater. Res. Soc. Symp. Proc. **2007**, 980.
[8]M. F. X. Wagner and W. Windl, Acta Mater. **56**, 6232 (2008).
[9]X. Huang, G. Ackland, and K. Rabe, Nat. Mater. **2**, 307 (2003).
[10]M. Nishida, K. Yamauchi, I. Itai, H. Ohgi, and A. Chiba, Acta Metall. Mater. **43**, 1229 (1995).
[11]M. Nishida, H. Ohgi, I. Itai, A. Chiba, and K. Yamauchi, Acta Metall. Mater. **43**, 1219 (1995).
[12]T. Onda, Y. Bando, T. Ohba, and K. Otsuka, Mater. Trans., JIM **33**, 354 (1992).
[13]T. Waitz, D. Spisak, J. Hafner, and H. P. Karnthaler, Europhys. Lett. **71**, 98 (2005).
[14]P. Šesták, M. Černý, and J. Pokluda, Intermetallics **19**, 1567 (2011).
[15]Y. Zhong, K. Gall, and T. Zhu, J. Appl. Phys. **110**, 033532 (2011).
[16]G. Kresse and J. Hafner, Phys. Rev. B **48**, 13115 (1993).
[17]G. Kresse and J. Furthmuller, Phys. Rev. B **54**, 11169 (1996).
[18]K. G. Vishnu and A. Strachan, Phys. Rev. B **85**, 014114 (2012).
[19]D. Holec, M. Friák, A. Dlouhý, and J. Neugebauer, Phys. Rev. B **84**, 224119 (2011).
[20]P. Šittner, P. Lukáš, V. Novák, M. R. Daymond, and G. M. Swallowe, Mater. Sci. Eng. A **378**, 97 (2004).